

Efficient Transformed Gaussian Process State-Space Models for Non-Stationary High-Dimensional Dynamical Systems

Zhidi Lin[✉], Ying Li, Feng Yin[✉], *Senior Member, IEEE*, Juan Maroñas[✉], and Alexandre H. Thiéry[✉]

Abstract—Gaussian process state-space models (GPSSMs) offer a principled framework for learning and inference in nonlinear dynamical systems with uncertainty quantification. However, existing GPSSMs are limited by the use of multiple independent stationary Gaussian processes (GPs), leading to prohibitive computational and parametric complexity in high-dimensional settings and restricted modeling capacity for non-stationary dynamics. To address these challenges, we propose an efficient transformed Gaussian process state-space model (ETGPSSM) for scalable and flexible modeling of high-dimensional, non-stationary dynamical systems. Specifically, our ETGPSSM integrates a single shared GP with input-dependent normalizing flows, yielding an expressive implicit process prior that captures complex, non-stationary transition dynamics while significantly reducing model complexity. For the inference of the implicit process, we develop a variational inference algorithm that jointly approximates the posterior over the underlying GP and the neural network parameters defining the normalizing flows. To avoid explicit variational parameterization of the latent states, we further incorporate the ensemble Kalman filter (EnKF) into the variational framework, enabling accurate and efficient state estimation. Extensive empirical evaluations on synthetic and real-world datasets demonstrate the superior performance of our ETGPSSM in system dynamics learning, high-dimensional state estimation, and time-series forecasting, outperforming existing GPSSMs and neural network-based SSMs in terms of computational efficiency and accuracy.

Index Terms—Gaussian process, state-space model, normalizing flows, variational inference, high-dimensional dynamical systems.

I. INTRODUCTION

STATE-SPACE models (SSMs) offer a versatile framework for capturing dynamical systems where latent states evolve based on internal dynamics and external inputs [1]. For systems with well-defined dynamics, Bayesian filtering

methods—including the Kalman filter (KF), extended Kalman filter (EKF), ensemble Kalman filter (EnKF), and particle filter (PF)—enable sequential state estimation by integrating prior knowledge with new observations, thus facilitating reliable predictions in uncertain conditions. This capability makes SSMs highly applicable in fields such as robotics, finance, control systems, and signal processing, where modeling temporal dependencies is essential [2], [3], [4]. Yet, in many complex real-world scenarios, the lack of precise knowledge about system dynamics significantly limits traditional SSM methods, particularly for nonlinear, high-dimensional systems like climate models, physiological processes, robotics, and neural dynamics [5].

To address this challenge, numerous data-driven modeling and system identification approaches have been proposed. Deterministic models, such as deep state-space models (DSSMs), employ neural networks to learn system dynamics and have gained popularity for their ability to capture high-dimensional, nonlinear behaviors [6]. However, these models often demand extensive training datasets to mitigate overfitting, exhibit limited generalization in uncertain environments, and lack interpretability in their predictions [7]. Consequently, despite their theoretical potential, DSSMs frequently underperform in practical applications [8].

In contrast, stochastic models incorporating flexible random process priors offer a robust alternative within a Bayesian learning framework [9]. A prominent example is the class of Gaussian process state-space models (GPSSMs), which utilize Gaussian processes (GPs) to provide interpretable uncertainty quantification and inherent regularization, making them extraordinary for modeling safety-critical dynamical systems [10], [11]. Consequently, GPSSMs have been extensively utilized in various applications, including human pose and motion learning [12], robotics and control learning [13], reinforcement learning [14], [15], target tracking and navigation [16], and magnetic-field sensing [17].

Research on GPSSMs has also focused on advancing learning and inference methodologies. Early works either assumed a pre-learned GPSSM and concentrated solely on latent state inference—an impractical assumption for many real-world applications [18], [19], [20]—or employed maximum *a posteriori* (MAP) estimation to jointly infer the model and the latent states [12], [21], which is prone to overfitting. To address these issues, a pivotal development came with the fully Bayesian treatment of GPSSMs using particle Markov chain

Zhidi Lin and Alexandre H. Thiéry are with the the Department of Statistics and Data Science, National University of Singapore, Singapore 117546 (Email: zhidilin@nus.edu.sg, a.h.thiery@nus.edu.sg). Alexandre H. Thiéry is the corresponding author.

Ying Li is with the Department of Statistics and Actuarial Science, University of Hong Kong, Hong Kong, SAR, China (Email: lynnli98@connect.hku.hk).

Feng Yin is with the School of Science and Engineering, The Chinese University of Hong Kong, Shenzhen, Shenzhen 518172, China (Email: yin-feng@cuhk.edu.cn).

Juan Maroñas is with the Machine Learning Group, Universidad Autónoma de Madrid, and with the Department of Quantitative Methods at CUNEF Universidad (Email: juan.maronas@cunef.edu).

Monte Carlo (PMCMC) methods [22], though the inherent cubic computational complexity of GP remains prohibitive for long time series. Subsequent efforts [23], [24], [25], [26] adopted reduced-rank GP approximations to alleviate the computational demands, yet PMCMC scalability remains a challenge. This has led to a growing interest in variational inference methods [10], [27], [28], [29], [30], [31], [32], [33], [34], [35], [36], [37], [38], [39], which leverage sparse GP approximations with inducing points to enhance scalability [40], [41].

However, existing GPSSMs, which employ multiple independent GPs to model system dynamics, remain limited to low-dimensional state spaces and face fundamental challenges when scaling to high-dimensional systems. Specifically, in variational GPSSMs, the inherent cubic computational complexity of the GPs scales linearly with the state dimension, while the number of parameters grows quadratically. This computational and parametric complexity seriously hinders the applicability of GPSSMs to high-dimensional systems. Additionally, all GPSSMs inherit a fundamental limitation, namely the use of stationary random process priors for modeling system dynamics. Such stationary assumptions are often inadequate for capturing time-varying and complex transition functions, ultimately limiting GPSSMs' ability to model complex dynamical systems accurately.

To address these challenges, we propose a novel approach for learning and inference in GPSSMs tailored to non-stationary, high-dimensional dynamical systems. Our primary contribution is the development and integration of an efficient yet flexible implicit process prior [42] for the state transition function. This prior combines the strengths of GPs, normalizing flows [43], and (Bayesian) neural networks, significantly enhancing modeling capabilities in high-dimensional state spaces. Our key contributions are summarized as follows:

- Instead of employing multiple independent GPs for the transition function, we propose applying an efficient transformed Gaussian process (ETGP), an implicit random process that combines a shared GP with normalizing flows. Crucially, the flow parameters are made input-dependent through neural network modeling. This novel modeling approach offers two key advantages: (1) it captures complex, non-stationary transition functions that standard GP priors cannot represent, and (2) by utilizing only a single shared GP, it mitigates the computational and parametric complexities of traditional GPSSMs in high-dimensional spaces, enabling effective scaling to higher dimensions.
- For efficient inference, we develop a scalable variational algorithm to jointly approximate the posterior distributions of both the ETGP and the latent states. Unlike standard GPs, the implicit nature of the ETGP prevents direct parametrization of the function-space posterior. To address this challenge, we explicitly approximate the posterior over the underlying GP and the associated neural network parameters, which together define the ETGP posterior. Additionally, we incorporate the EnKF into the variational inference framework, eliminating the need to parameterize the variational distributions over

latent states. This hybrid formulation thus not only offers accurate state estimation but also substantially reduces the computational cost of the parameter optimization.

- Finally, extensive empirical evaluations across system dynamics learning, high-dimensional state estimation, and time-series prediction demonstrate the superiority of our proposed method. It achieves significantly lower computational and parametric complexity than conventional GPSSMs while outperforming state-of-the-art approaches, including deep neural network-based SSMs, in terms of learning and inference accuracy.

Part of this work was presented at IEEE ICASSP 2024 [38]. The current paper introduces input-dependent normalizing flows to further enhance model flexibility and proposes an EnKF-aided variational inference algorithm for efficient state estimation. More extensive empirical validations are also included to demonstrate the superiority of the proposed method.

The remainder of this paper is structured as follows. Section II introduces the preliminaries of state-space models and outlines key challenges in existing GPSSMs. Section III presents our proposed efficient GPSSM framework for high-dimensional dynamical systems, including the associated variational inference algorithm. Experimental results are detailed in Section IV, followed by concluding remarks in Section V. Technical proofs and derivations are deferred to the Appendix.

II. PRELIMINARIES

Section II-A introduces the SSM considered in this work. A brief review of GPSSM is presented in Section II-B. The challenges associated with existing GPSSMs are discussed in detail in Section II-C.

A. State-Space Models (SSMs)

A generic SSM describes the probabilistic relationship between the latent state $\mathbf{x}_t \in \mathbb{R}^{d_x}$ and the observation $\mathbf{y}_t \in \mathbb{R}^{d_y}$. It can be mathematically expressed as:

$$(\text{Transition}): \quad \mathbf{x}_{t+1} = \mathbf{f}(\mathbf{x}_t) + \mathbf{v}_t, \quad \mathbf{v}_t \sim \mathcal{N}(\mathbf{0}, \mathbf{Q}), \quad (1a)$$

$$(\text{Emission}): \quad \mathbf{y}_t = \mathbf{C}\mathbf{x}_t + \mathbf{e}_t, \quad \mathbf{e}_t \sim \mathcal{N}(\mathbf{0}, \mathbf{R}). \quad (1b)$$

Here, the latent states follow a Markov process, meaning that at any time step $t \in \mathbb{N}$, the next state \mathbf{x}_{t+1} depends only on the current state \mathbf{x}_t and the transition function $\mathbf{f}(\cdot) : \mathbb{R}^{d_x} \mapsto \mathbb{R}^{d_x}$. In this paper, the emission function is assumed to be linear, with the coefficient matrix $\mathbf{C} \in \mathbb{R}^{d_y \times d_x}$. For systems with nonlinear emission functions, the latent state can be augmented to a higher dimension, transforming the system into one with a linear emission function [30], which mitigates the non-identifiability issues commonly encountered in data-driven SSMs [10]. Both the latent states and observations are assumed to be perturbed by zero-mean Gaussian noise, with covariance matrices \mathbf{Q} and \mathbf{R} , respectively.

B. Gaussian Process State-Space Models (GPSSMs)

As discussed in Section I, system dynamics in real-world complex scenarios are often unknown, with only a set of noisy observations, $\mathbf{y}_{1:T} = \{\mathbf{y}_t\}_{t=1}^T$, available. Consequently, there

has been growing interest in adopting data-driven approaches, such as GPs [9], to model these dynamics and quantify the underlying uncertainties.

1) **Gaussian process (GP)**: The GP is a generalization of the Gaussian distribution over infinite index sets, enabling the specification of distributions over functions $\tilde{f}(\cdot) : \mathbb{R}^{d_x} \mapsto \mathbb{R}$. A GP is fully characterized by its mean function, often set to zero, and its covariance (kernel) function $k(\mathbf{x}, \mathbf{x}')$, which includes a set of hyperparameters θ_{gp} that need to be optimized for model selection [9]. According to the definition of a GP, the function values $\tilde{\mathbf{f}} = \{\tilde{f}(\mathbf{x}_i)\}_{i=1}^N \in \mathbb{R}^N$ at any finite set of points $\mathbf{X} = \{\mathbf{x}_i\}_{i=1}^N \in \mathbb{R}^{N \times d_x}$ follow a joint Gaussian distribution, i.e.,

$$p(\tilde{\mathbf{f}} | \mathbf{X}) = \mathcal{N}(\tilde{\mathbf{f}} | \mathbf{0}, \mathbf{K}), \quad (2)$$

where $\mathbf{K} \in \mathbb{R}^{N \times N}$ is the covariance matrix evaluated on the finite input \mathbf{X} with $[\mathbf{K}]_{i,j} = k(\mathbf{x}_i, \mathbf{x}_j)$.

Given the observed function values $\tilde{\mathbf{f}}$ at the input \mathbf{X} , the GP prediction distribution, $p(\tilde{f}(\mathbf{x}_*) | \tilde{\mathbf{f}}, \mathbf{X})$, at any new input \mathbf{x}_* , is also Gaussian, and fully characterized by the posterior mean $\xi(\mathbf{x}_*)$ and the posterior variance $\Xi(\mathbf{x}_*)$. Concretely,

$$\xi(\mathbf{x}_*) = \mathbf{K}_{\mathbf{x}_*, \mathbf{X}} \mathbf{K}^{-1} \tilde{\mathbf{f}}, \quad (3a)$$

$$\Xi(\mathbf{x}_*) = k(\mathbf{x}_*, \mathbf{x}_*) - \mathbf{K}_{\mathbf{x}_*, \mathbf{X}} \mathbf{K}^{-1} \mathbf{K}_{\mathbf{X}, \mathbf{x}_*}^\top, \quad (3b)$$

where $\mathbf{K}_{\mathbf{x}_*, \mathbf{X}}$ is the cross covariance matrix evaluated on the new input \mathbf{x}_* and the observed input \mathbf{X} .

2) **Gaussian process state-space model**: Placing a GP prior over the transition function $\mathbf{f}(\cdot)$ in the classic SSM (see Eq. (1)) leads to the following salient GPSSM [10]:

$$\mathbf{f}(\cdot) \sim \mathcal{GP}(\mathbf{0}, k(\cdot, \cdot)), \quad (4a)$$

$$\mathbf{f}_t = \mathbf{f}(\mathbf{x}_{t-1}), \quad (4b)$$

$$\mathbf{x}_0 \sim p(\mathbf{x}_0), \quad (4c)$$

$$\mathbf{x}_t | \mathbf{f}_t \sim \mathcal{N}(\mathbf{x}_t | \mathbf{f}_t, \mathbf{Q}), \quad (4d)$$

$$\mathbf{y}_t | \mathbf{x}_t \sim \mathcal{N}(\mathbf{y}_t | \mathbf{C}\mathbf{x}_t, \mathbf{R}), \quad (4e)$$

where the initial state prior distribution $p(\mathbf{x}_0)$ is assumed to be known and follows a Gaussian distribution. The graphical representation is depicted in Fig. 1.

In GPSSMs, when the state dimension $d_x > 1$, the transition $\mathbf{f}(\cdot) : \mathbb{R}^{d_x} \mapsto \mathbb{R}^{d_x}$ is typically modeled using d_x mutually independent GPs. Each independent GP represents a dimension-specific function $f_d(\cdot) : \mathbb{R}^{d_x} \mapsto \mathbb{R}$, and the multivariate output is expressed as

$$\mathbf{f}_t = \mathbf{f}(\mathbf{x}_{t-1}) = \{f_d(\mathbf{x}_{t-1})\}_{d=1}^{d_x} = \{\mathbf{f}_{t,d}\}_{d=1}^{d_x}, \quad (5)$$

where each independent GP is characterized by a distinct kernel function and associated hyperparameters [30]. The main challenge in GPSSMs is the simultaneous learning of the transition function and noise parameters, i.e., learning $[\theta_{gp}, \mathbf{Q}, \mathbf{R}]$, while inferring both the GPs and the latent states of interest.

C. Challenges in Existing Variational GPSSMs

Note that in Eq. (3), evaluating the GP posterior involves inverting the covariance matrix \mathbf{K} , resulting in a computational

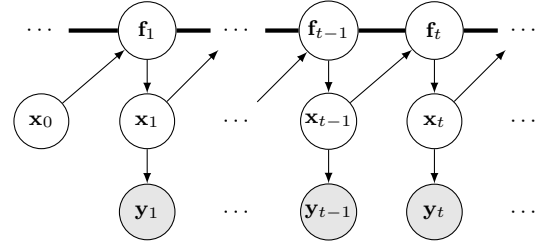


Fig. 1: Graphical representation of GPSSM. The white circles represent the latent variables, while the gray circles represent the observable variables. The thick horizontal bar represents a set of fully connected, mutually correlated nodes, specifically, the GP.

cost of $\mathcal{O}(N^3)$, which becomes prohibitive for large N . To address this issue, variational GPSSMs typically adopt sparse GP approximations [40], [41], a ubiquitous technique in GP-based models [44], [10] due to its analytical and computational tractability. The general idea of the sparse GP involves augmenting the corresponding GP by introducing a set of inducing points $\mathbf{Z} = \{\mathbf{z}_i\}_{i=1}^M$ and $\mathbf{u} = \{\mathbf{u}_i\}_{i=1}^M$, $M \ll N$, that will serve as a surrogate for the GP. Here, $\mathbf{u} \sim \mathcal{N}(\mathbf{0}, \mathbf{K}_{\mathbf{Z}, \mathbf{Z}})$ and $\mathbf{z}_i \in \mathbb{R}^{d_x}$. Specifically, the augmented GP prior is given by¹,

$$p(\tilde{f}, \mathbf{u}) = p(\tilde{f} | \mathbf{u}) p(\mathbf{u}). \quad (6)$$

We can approximate the corresponding GP posterior by explicitly specifying a free Gaussian density on the function values \mathbf{u} at M locations, $q(\mathbf{u}) = \mathcal{N}(\mathbf{u} | \mathbf{m}, \mathbf{S})$, and using the prior conditional for the rest of the GP, i.e.,

$$q(\tilde{f}, \mathbf{u}) = p(\tilde{f} | \mathbf{u}) q(\mathbf{u}). \quad (7)$$

This leads to an explicit form for the approximate GP posterior

$$q(\tilde{f}) = \int q(\tilde{f}, \mathbf{u}) d\mathbf{u} = \mathcal{N}(\tilde{f}(\mathbf{x}_*) | \xi_p(\mathbf{x}_*), \Xi_p(\mathbf{x}_*)), \quad (8)$$

where

$$\xi_p(\mathbf{x}_*) = \mathbf{K}_{\mathbf{x}_*, \mathbf{Z}} \mathbf{K}_{\mathbf{Z}, \mathbf{Z}}^{-1} \mathbf{m}, \quad (9a)$$

$$\Xi_p(\mathbf{x}_*) = \mathbf{K}_{\mathbf{x}_*, \mathbf{x}_*} - \mathbf{K}_{\mathbf{x}_*, \mathbf{Z}} \mathbf{K}_{\mathbf{Z}, \mathbf{Z}}^{-1} [\mathbf{K}_{\mathbf{Z}, \mathbf{Z}} - \mathbf{S}] \mathbf{K}_{\mathbf{Z}, \mathbf{Z}}^{-1} \mathbf{K}_{\mathbf{x}_*, \mathbf{Z}}^\top, \quad (9b)$$

resulting in a computational complexity that scales as $\mathcal{O}(M^3)$ instead of $\mathcal{O}(N^3)$.

Nevertheless, existing variational GPSSMs still face significant computational and modeling challenges, which are listed below.

- Modeling multi-dimensional state transition function using multiple separate GP results in a computational complexity of $\mathcal{O}(d_x M^3)$ in GPSSMs, where the complexity grows linearly with the latent state dimension d_x .
- The variational approximation of the GP posterior introduces a number of variational parameters that scale quadratically with the state dimensionality d_x . Specifically, the variational parameters in multi-dimensional GPSSMs include inducing inputs $\{\mathbf{Z}_d\}_{d=1}^{d_x} \in \mathbb{R}^{d_x \times (M \times d_x)}$, variational means $\{\mathbf{m}_d\}_{d=1}^{d_x} \in \mathbb{R}^{d_x \times M}$, and covariance matrices $\{\mathbf{S}_d\}_{d=1}^{d_x} \in \mathbb{R}^{d_x \times (M \times M)}$ for the

¹With slight notation abuse, we denote the distribution of GP prior as $p(\tilde{f})$.

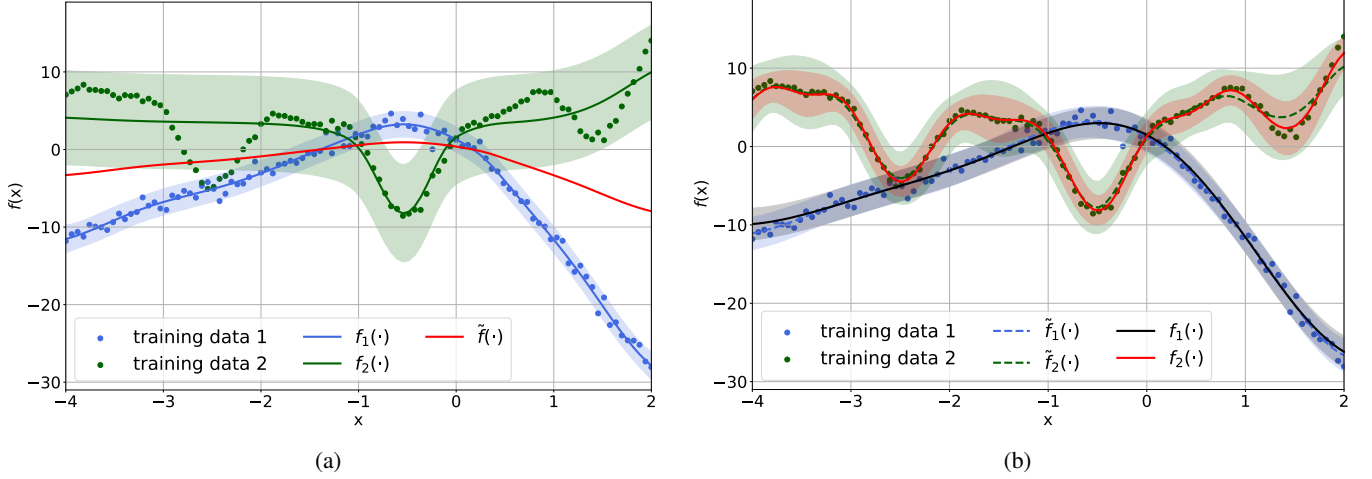


Fig. 2: **(a)** Two warped GPs, see Eq. (10). $f_1(\cdot)$ effectively fits the data, while $f_2(\cdot)$ falls short. **(b)** Independent GPs ($\tilde{f}_1(\cdot)$, $\tilde{f}_2(\cdot)$) vs our proposed ETGP ($f_1(\cdot)$, $f_2(\cdot)$) from Fig. 3. Both methods capture the underlying function reasonably well, though the GP $\tilde{f}_1(\cdot)$ exhibits slightly worse fit and overestimated uncertainty.

d_x -dimensional inducing outputs $\{\mathbf{u}_d\}_{d=1}^{d_x}$. As the state dimension increases, the quadratic scaling of inducing inputs can lead to computational intractability, while the scaling of the variational means and covariance matrices further compounds the computational burden [38].

- Existing GPSSMs commonly place a stationary GP prior over the transition function, as shown in Eq. (4a), to model a time-invariant transition function. However, this approach may fail to adequately capture non-stationary dynamics, leading to inaccuracies in scenarios where the transition function evolves over time. Moreover, the use of independent GPs for each dimension of the transition function overlooks dependencies between outputs.

In the next section, we detail our proposed method to resolve these issues.

III. EFFICIENT TRANSFORMED GAUSSIAN PROCESS STATE-SPACE MODELS

We first introduce the proposed efficient and flexible modeling framework for high-dimensional state spaces in Section III-A. Section III-B then presents the corresponding Bayesian variational inference algorithm. Finally, the details of EnKF-aided variational lower bound evaluation are provided in Section III-C.

A. Efficient Modeling for High-Dimensional State Space

In Section II-C, we discussed the computational and modeling challenges associated with using separate GPs for each dimension of the transition function in high-dimensional state spaces. To address these issues, in [38], we proposed to warp a single shared GP using normalizing flows [43] to fit each dimension of the transition function, that is,

$$\tilde{f}(\cdot) \sim \mathcal{GP}(0, k(\cdot, \cdot)), \quad f_d(\cdot) = \mathbb{G}_{\theta_d}(\tilde{f}(\cdot)), \quad d=1, \dots, d_x, \quad (10)$$

where each dimension-specific normalizing flow, $\mathbb{G}_{\theta_d}(\cdot)$, is an element-wise, invertible and differentiable (bijective) function

parameterized by $\theta_d \in \Theta$. Two specific examples are provided below.

Example 1. If $\mathbb{G}_{\theta_d}(\cdot)$ is a simple linear flow, then we have

$$f_d(\cdot) = \alpha_d \cdot \tilde{f}(\cdot) + \beta_d,$$

with $\theta_d = [\alpha_d, \beta_d]^\top \in \mathbb{R}^2$.

Example 2. If $\mathbb{G}_{\theta_d}(\cdot)$ is a Sinh-Arcsinh-Linear (SAL) flow [44], [45], we have:

$$f_d(\cdot) = \alpha_d \sinh \left[\varphi_d \operatorname{arcsinh} \left(\tilde{f}(\cdot) \right) - \gamma_d \right] + \beta_d,$$

with $\theta_d = [\alpha_d, \beta_d, \gamma_d, \varphi_d]^\top \in \mathbb{R}^4$.

More complex flows can be achieved by stacking additional layers of SAL flow and/or incorporating more advanced deep neural network-based flows, such as RealNVP [46].

The primary advantage of this methodology lies in its elimination of multiple independent GPs by leveraging computationally efficient flow transformations, thereby enabling circumvent the $\mathcal{O}(d_x M^3)$ computational complexity and quadratic parameter proliferation mentioned in Section II-C. Additionally, the warped GPs are dependent which could potentially alleviate the limitation of independence modeling in conventional GPSSMs.

However, the warped GP in Eq. (10) remains stationary and, being based on a single GP, may still lack the flexibility required to capture complex latent state dynamics, leading to suboptimal learning performance [38]. An intuitive illustrative example is shown in Fig. 2a, where the learned element-wise flow \mathbb{G}_{θ_1} successfully warps \tilde{f} to obtain f_1 , achieving accurate fitting of the underlying function's simple pattern. However, when faced with more complex, non-stationary data trajectories, the warped GP, f_2 , struggles to capture these patterns, resulting in huge modeling uncertainty. For a more comprehensive comparison, Fig. 2b also presents the fitting results obtained using two independent GPs and the ETGP model introduced later in this paper. Both methods effec-

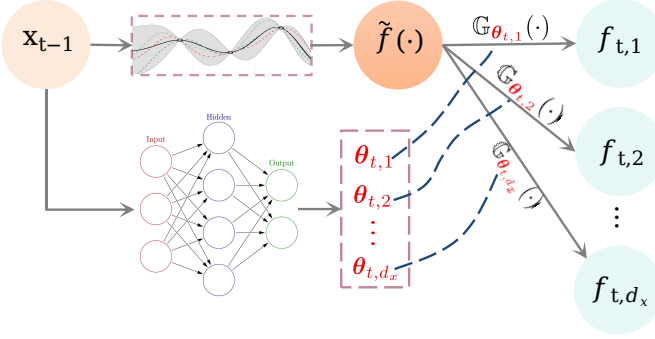


Fig. 3: ETGP transition function in SSMs

tively capture the underlying functions, although the GP $\tilde{f}_1(\cdot)$ demonstrates a slightly inferior fit and inflated uncertainty estimates, due to its inherent stationarity.

To address the limitations in modeling flexibility exhibited by existing methods, we draw inspiration from recent advances in adaptive parameterization [44], [47] and introduce non-stationarity and input dependence into the warped GPs. Specifically, we generate non-stationary processes $\{f_d(\cdot)\}_{d=1}^{d_x}$ by making the flow parameters depend on the input through a shallow neural network, denoted as $\text{NN} : \mathbb{R}^{d_x} \mapsto \Theta$ and parameterized by a weight vector \mathbf{w} . Formally, in the context of SSM, this is expressed as²:

$$\boldsymbol{\theta}_t = \text{NN}_{\mathbf{w}}(\mathbf{x}_{t-1}), \quad (11)$$

where $\boldsymbol{\theta}_t = \{\theta_{t,d}\}_{d=1}^{d_x}$. In this case, the flow parameters vary with the input at each time step t , enabling the capture of local variation patterns and facilitating the modeling of time-varying transition functions. Additionally, note that the parameter amortization learning shown in Eq. (11) can avoid that the number of flow parameters increases linearly with time step t . Moreover, sharing neural network parameters across flow parameterizations further improves modeling efficiency.

We may further impose a prior $p_{\psi}(\mathbf{w})$ over \mathbf{w} with hyperparameter ψ (e.g., $\mathbf{w} \sim \mathcal{N}(\mathbf{w}|\mathbf{0}, \text{diag}(\psi))$) to regularize the neural network's parameters and mitigate overfitting issues. In summary, our modeling approach can be expressed mathematically as follows:

$$\tilde{f}(\cdot) \sim \mathcal{GP}(0, k(\cdot, \cdot)), \quad \mathbf{w} \sim p_{\psi}(\mathbf{w}), \quad (12a)$$

$$\boldsymbol{\theta}_t = \text{NN}_{\mathbf{w}}(\mathbf{x}_{t-1}), \quad f_d(\cdot) = \mathcal{G}_{\boldsymbol{\theta}_{t,d}}(\tilde{f}(\cdot)), \quad d=1, \dots, d_x, \quad (12b)$$

where $\{f_d(\cdot)\}_{d=1}^{d_x}$ implicitly characterize d_x random processes [42]. To better understand the modeling, Fig. 3 illustrates the corresponding graphical representation with $p_{\psi}(\mathbf{w}) = \delta(\mathbf{w} - \bar{\mathbf{w}})$, where $\delta(\cdot)$ is the Dirac delta measure and $\bar{\mathbf{w}}$ is a deterministic vector, and the following example extends the Example 1, providing a more concrete illustration.

Example 3. In the case of the linear flow, we have

$$\mathbf{f}(\cdot) = \boldsymbol{\alpha}_t \cdot \tilde{f}(\cdot) + \boldsymbol{\beta}_t, \quad (13a)$$

$$\boldsymbol{\theta}_t = \text{NN}_{\mathbf{w}}(\mathbf{x}_{t-1}), \quad \mathbf{w} \sim p_{\psi}(\mathbf{w}). \quad (13b)$$

where $\boldsymbol{\theta}_t = [\boldsymbol{\alpha}_t^{\top}, \boldsymbol{\beta}_t^{\top}]^{\top}$, and $\boldsymbol{\alpha}_t = \{\alpha_{t,d}\}_{d=1}^{d_x}$, $\boldsymbol{\beta}_t = \{\beta_{t,d}\}_{d=1}^{d_x}$. An illustrative example of function fitting using the ETGP with linear flows is depicted in Fig. 2b.

It is noteworthy that this modeling approach, also known as the efficient transformed Gaussian process (ETGP) in the GP literature, was initially proposed to address large-scale multi-class classification problems [48]. The efficiency stems from the use of a single GP rather than multiple GPs for multi-class settings, thereby ensuring that the computational cost of GP operations remains constant with respect to the number of classes. This leads to a substantial reduction in overall computations. In this work, we adapt it to model the high-dimensional transition function in SSMs. Additionally, ETGP implicitly characterizes d_x dependent random processes [42], a dependence that has been overlooked in prior GPSSM literature. A more detailed insight is provided below.

Corollary 1. If $p_{\psi}(\mathbf{w}) = \delta(\mathbf{w} - \bar{\mathbf{w}})$, where $\bar{\mathbf{w}}$ is a deterministic vector, then the ETGP defined in Example 3 becomes a d_x -dimensional dependent non-stationary Gaussian process with time-dependent covariance. Specifically, at arbitrary time steps t and t' , we have

$$\begin{bmatrix} \mathbf{f}(\mathbf{x}_{t-1}) \\ \mathbf{f}(\mathbf{x}_{t'-1}) \end{bmatrix} \sim \mathcal{N} \left(\begin{bmatrix} \boldsymbol{\beta}_t \\ \boldsymbol{\beta}_{t'} \end{bmatrix}, \boldsymbol{\Lambda}_{t,t'} \right), \quad (14)$$

where the covariance matrix $\boldsymbol{\Lambda}_{t,t'} \in \mathbb{R}^{2d_x \times 2d_x}$ is given by

$$\boldsymbol{\Lambda}_{t,t'} = \begin{bmatrix} k(\mathbf{x}_{t-1}, \mathbf{x}_{t-1}) \cdot \boldsymbol{\alpha}_t \boldsymbol{\alpha}_t^{\top} & k(\mathbf{x}_{t-1}, \mathbf{x}_{t'-1}) \cdot \boldsymbol{\alpha}_t \boldsymbol{\alpha}_{t'}^{\top} \\ k(\mathbf{x}_{t'-1}, \mathbf{x}_{t-1}) \cdot \boldsymbol{\alpha}_{t'} \boldsymbol{\alpha}_t^{\top} & k(\mathbf{x}_{t'-1}, \mathbf{x}_{t'-1}) \cdot \boldsymbol{\alpha}_{t'} \boldsymbol{\alpha}_{t'}^{\top} \end{bmatrix}. \quad (15)$$

Proof. This result can be built upon the Gaussianity and the linearity property of covariance, which can be found in Appendix A. \square

With the computationally efficient and flexible function prior defined by ETGP $\mathbf{f}(\cdot) = \{f_d(\cdot)\}_{d=1}^{d_x}$, we can define our proposed SSM, termed ETGPSSM, compactly expressed as follows:

$$\mathbf{f}(\cdot) \sim \mathcal{ETGP}(\tilde{f}(\cdot), p_{\psi}(\mathbf{w})), \quad (16a)$$

$$\mathbf{x}_0 \sim p(\mathbf{x}_0), \quad (16b)$$

$$\mathbf{f}_t = \mathbf{f}(\mathbf{x}_{t-1}), \quad (16c)$$

$$\mathbf{x}_t | \mathbf{f}_t \sim \mathcal{N}(\mathbf{x}_t | \mathbf{f}_t, \mathbf{Q}), \quad (16d)$$

$$\mathbf{y}_t | \mathbf{x}_t \sim \mathcal{N}(\mathbf{y}_t | \mathbf{C} \mathbf{x}_t, \mathbf{R}), \quad (16e)$$

where the ETGP prior is characterized by the associated GP $\tilde{f}(\cdot)$, neural network weight prior $p_{\psi}(\mathbf{w})$, and the normalizing flows, see Eq. (12). In this paper, unless otherwise specified, we focus on the linear flow shown in Example 3 for simplicity and illustrative purposes. Additionally, the linear flow requires learning only 2 parameters per dimension, making it more efficient compared to other types of normalizing flows. We also assume that the prior distribution of the initial state, $p(\mathbf{x}_0)$, is Gaussian and known for simplicity.

²Note that \mathbf{x}_t can always be extended to accommodate control systems incorporating a deterministic control input $\mathbf{c}_t \in \mathbb{R}^{d_c}$ by augmenting the latent state to $[\mathbf{x}_t^{\top}, \mathbf{c}_t^{\top}]^{\top} \in \mathbb{R}^{d_x+d_c}$. For brevity, however, we omit explicit reference to \mathbf{c}_t in our notation throughout this paper.

Remark 1. In contrast to existing GPSSMs, the $\{f_d(\cdot)\}_{d=1}^{d_x}$ in the ETGPSSM are dependent, as they are both transformed random processes derived from a shared GP and common weight priors (see Corollary 1). Furthermore, as these induced random processes are non-stationary (see Corollary 1), they are well-suited for modeling time-varying transition functions.

The primary objective in ETGPSSM, as in GPSSM, is the joint estimation of model hyperparameters $\vartheta = \{\theta_{gp}, \psi, \mathbf{Q}, \mathbf{R}\}$ and inference of both the ETGP and latent states. More specifically, given a sequence of observations $\mathbf{y}_{1:T} = \{\mathbf{y}_t\}_{t=1}^T$, with $T \in \mathbb{Z}_+$, the task is to estimate ϑ and compute the posterior distributions $p(\mathbf{f}(\cdot) | \mathbf{y}_{1:T})$ for the ETGP and $p(\mathbf{x}_{0:T} | \mathbf{y}_{1:T})$ for the latent states, where $\mathbf{x}_{0:T} = \{\mathbf{x}_t\}_{t=0}^T$.

However, the marginal likelihood $p(\mathbf{y}_{1:T} | \vartheta)$ is generally intractable, rendering both hyperparameter estimation via model evidence maximization and posterior inference computationally infeasible. Furthermore, unlike standard GPs that admit closed-form expressions for the prior and posterior distributions (see Eqs. (2) and (3)), the ETGP constitutes an implicit stochastic process. Consequently, the marginal prior³ and posterior distributions are analytically intractable [42], posing significant challenges for inference. The next subsections introduce a variational inference framework that enables joint learning of model hyperparameters and Bayesian inference of the ETGP and latent states.

B. Approximate Bayesian Inference

To address the intractability of the marginal distribution $p(\mathbf{y}_{1:T} | \vartheta)$, we resort to variational inference, which involves maximizing an evidence lower bound (ELBO) on the logarithm of the marginal likelihood [49]. The ELBO, denoted as \mathcal{L} , can be generally constructed as follows:

$$\mathcal{L} = \mathbb{E}_{q(\mathbf{x}_{0:T}, \mathbf{f}(\cdot))} \left[\log \frac{p(\mathbf{y}_{1:T}, \mathbf{x}_{0:T}, \mathbf{f}(\cdot))}{q(\mathbf{x}_{0:T}, \mathbf{f}(\cdot))} \right], \quad (17)$$

so that the difference between $\log p(\mathbf{y}_{1:T} | \vartheta)$ and \mathcal{L} equals the Kullback-Leibler (KL) divergence between the introduced variational approximation $q(\mathbf{x}_{0:T}, \mathbf{f}(\cdot))$ and the true posterior $p(\mathbf{x}_{0:T}, \mathbf{f}(\cdot) | \mathbf{y}_{1:T})$. We then can jointly maximize \mathcal{L} with respect to ϑ and the variational distribution $q(\mathbf{x}_{0:T}, \mathbf{f}(\cdot))$ to obtain the model hyperparameter estimates and the approximation of the posterior distribution $p(\mathbf{x}_{0:T}, \mathbf{f}(\cdot) | \mathbf{y}_{1:T})$.

However, as noted earlier, the absence of closed-form expressions for the ETGP's prior and posterior distributions prevents direct expansion of the ELBO in Eq. (17). To address this challenge, rather than operating in the function space of the ETGP, we instead follow its generative construction—illustrated in Fig. 3—and infer the posterior distributions over $\tilde{\mathbf{f}}$ and \mathbf{w} , which collectively characterize the ETGP posterior. Specifically, by explicitly representing $\tilde{\mathbf{f}}$ and \mathbf{w} , the joint distribution of the proposed ETGPSSM is given by:

$$p(\mathbf{y}_{1:T}, \mathbf{x}_{0:T}, \mathbf{w}, \tilde{\mathbf{f}}) = p(\mathbf{y}_{1:T}, \mathbf{x}_{0:T} | \mathbf{w}, \tilde{\mathbf{f}}) p_\psi(\mathbf{w}) p(\tilde{\mathbf{f}}), \quad (18)$$

where $p(\tilde{\mathbf{f}})$ represents the GP prior with a bit of notation abuse [31] and the prior of \mathbf{w} is assumed to be Gaussian,

$p_\psi(\mathbf{w}) = \mathcal{N}(\mathbf{w} | \mathbf{0}, \text{diag}(\psi))$, with diagonal variance. The term $p(\mathbf{y}_{1:T}, \mathbf{x}_{0:T} | \mathbf{w}, \tilde{\mathbf{f}})$ is factorized as:

$$p(\mathbf{y}_{1:T}, \mathbf{x}_{0:T} | \mathbf{w}, \tilde{\mathbf{f}}) = p(\mathbf{x}_0) \prod_{t=1}^T \underbrace{p(\mathbf{y}_t | \mathbf{x}_t)}_{\text{likelihood}} \underbrace{p(\mathbf{x}_t | \mathbf{w}, \tilde{\mathbf{f}}, \mathbf{x}_{t-1})}_{\text{transition}}, \quad (19)$$

where the transition term is specified as:

$$\begin{aligned} p(\mathbf{x}_t | \mathbf{w}, \tilde{\mathbf{f}}, \mathbf{x}_{t-1}) &= \int p(\mathbf{x}_t | \mathbf{f}_t) p(\mathbf{f}_t | \mathbf{w}, \tilde{\mathbf{f}}, \mathbf{x}_{t-1}) d\mathbf{f}_t \\ &= \mathcal{N}(\mathbf{x}_t | \boldsymbol{\alpha}_t \cdot \tilde{\mathbf{f}}(\mathbf{x}_{t-1}) + \boldsymbol{\beta}_t, \mathbf{Q}), \end{aligned} \quad (20)$$

with $p(\mathbf{f}_t | \mathbf{w}, \tilde{\mathbf{f}}, \mathbf{x}_{t-1}) = \delta(\mathbf{f}_t - (\boldsymbol{\alpha}_t \cdot \tilde{\mathbf{f}}(\mathbf{x}_{t-1}) + \boldsymbol{\beta}_t))$, and $\{\boldsymbol{\alpha}_t, \boldsymbol{\beta}_t\}$ being the outputs of the neural network parameterized by \mathbf{w} .

To infer the latent variables $\{\mathbf{x}_{0:T}, \mathbf{w}\}$ and the GP $\tilde{\mathbf{f}}$, we employ the following variational distribution:

$$q(\mathbf{x}_{0:T}, \tilde{\mathbf{f}}, \mathbf{w}) = q(\tilde{\mathbf{f}}), q(\mathbf{w}), q(\mathbf{x}_0) \prod_{t=1}^T q(\mathbf{x}_t | \mathbf{w}, \tilde{\mathbf{f}}, \mathbf{x}_{t-1}), \quad (21)$$

which mirrors the generative structure of the model in Eq. (18) and assumes independence between $\tilde{\mathbf{f}}$ and \mathbf{w} . Here the variational distributions of \mathbf{x}_0 and \mathbf{w} are defined as follows:

$$\begin{cases} q(\mathbf{x}_0) = \mathcal{N}(\mathbf{x}_0 | \mathbf{m}_0, \mathbf{L}_0 \mathbf{L}_0^\top), \\ q(\mathbf{w}) = \mathcal{N}(\mathbf{w} | \mathbf{m}_w, \text{diag}(\boldsymbol{\sigma}_w^2)), \end{cases} \quad (22)$$

where $\mathbf{m}_0 \in \mathbb{R}^{d_x}$, lower-triangular matrix $\mathbf{L}_0 \in \mathbb{R}^{d_x \times d_x}$, and $\{\mathbf{w}, \boldsymbol{\sigma}_w^2\}$ are free variational parameters.

For the variational distribution $q(\tilde{\mathbf{f}})$, we adopt a sparse GP approximation [40], [41], as defined in Eq. (8), which helps to reduce the computational complexity from $\mathcal{O}(T^3)$ to $\mathcal{O}(M^3)$.

For $q(\mathbf{x}_t | \mathbf{w}, \tilde{\mathbf{f}}, \mathbf{x}_{t-1})$ in Eq. (21), rather than assuming a parameterized form—which would introduce additional variational parameters and hence increase optimization complexity [31]—we draw inspiration from recent works [37], [50] and incorporate the EnKF into the variational learning framework to infer the latent states (see the next subsection for details). Specifically, without explicitly defining the variational distribution, we adopt the following approximation:

Assumption 1.

$$q(\mathbf{x}_t | \mathbf{w}, \tilde{\mathbf{f}}, \mathbf{x}_{t-1}) \approx p(\mathbf{x}_t | \mathbf{w}, \tilde{\mathbf{f}}, \mathbf{x}_{t-1}, \mathbf{y}_{1:t}), \quad (23)$$

which assumes that the variational distribution of \mathbf{x}_t can be approximated by the corresponding filtering distribution. Additionally, we assume that the following filtering distribution is approximately equal to its one-step backward smoothing counterpart, i.e.,

Assumption 2.

$$p(\mathbf{x}_{t-1} | \mathbf{w}, \tilde{\mathbf{f}}, \mathbf{y}_{1:t-1}) \approx p(\mathbf{x}_{t-1} | \mathbf{w}, \tilde{\mathbf{f}}, \mathbf{y}_{1:t}), \quad (24)$$

The two assumptions are reasonable and detailed justification can be found in Appendix B.

With these two assumptions, we can significantly streamline the evaluation of the ELBO, which is summarized in the following proposition.

³Obtaining $p(\mathbf{f}(\cdot))$ by marginalizing over the GP and \mathbf{w} is generally intractable.

Proposition 1. Under the two approximations, and all the assumed variational distributions, together with the model joint distribution in Eq. (18), the ELBO can be reformulated as follows:

$$\mathcal{L} \approx \mathbb{E}_{q(\mathbf{w}, \tilde{f})} \left[\sum_{t=1}^T \log p(\mathbf{y}_t | \mathbf{y}_{1:t-1}, \mathbf{w}, \tilde{f}) \right] - \text{KL}(q(\mathbf{u}) \| p(\mathbf{u})) - \text{KL}(q(\mathbf{w}) \| p(\mathbf{w})) - \text{KL}(q(\mathbf{x}_0) \| p(\mathbf{x}_0)), \quad (25)$$

where the first term (log-likelihood) can be analytically evaluated using the EnKF (detailed in Section III-C). The three KL divergence terms can also be computed in closed form, due to the Gaussian nature of the prior and variational distributions [49].

Proof. The proof can be found in Appendix B. \square

C. EnKF-aided ELBO Evaluation

We now demonstrate how to evaluate $p(\mathbf{y}_t | \mathbf{y}_{1:t-1}, \mathbf{w}, \tilde{f})$ in Eq. (25) using the EnKF. The general idea can be derived from Bayesian filtering. We first notice that

$$p(\mathbf{y}_t | \mathbf{y}_{1:t-1}, \mathbf{w}, \tilde{f}) = \int p(\mathbf{y}_t | \mathbf{x}_t) p(\mathbf{x}_t | \mathbf{w}, \tilde{f}, \mathbf{y}_{1:t-1}) d\mathbf{x}_t, \quad (26)$$

where the prediction distribution, $p(\mathbf{x}_t | \mathbf{w}, \tilde{f}, \mathbf{y}_{1:t-1}) =$

$$\int \underbrace{p(\mathbf{x}_t | \mathbf{w}, \tilde{f}, \mathbf{x}_{t-1})}_{\text{transition}} \underbrace{p(\mathbf{x}_{t-1} | \mathbf{w}, \tilde{f}, \mathbf{y}_{1:t-1})}_{\text{filtering}} d\mathbf{x}_{t-1}. \quad (27)$$

Consequently, we employ the EnKF, a widely used method for handling nonlinearities and high-dimensional state spaces [51], to obtain the filtering distribution $p(\mathbf{x}_t | \mathbf{w}, \tilde{f}, \mathbf{y}_{1:t})$ at each time step t . Further details are provided below.

1) **Prediction:** Given the ensemble of states $\{\mathbf{x}_{t-1}^{(i)}\}_{i=1}^N$ from the posterior distribution $p(\mathbf{x}_{t-1} | \mathbf{w}, \tilde{f}, \mathbf{y}_{1:t-1})$ at time $t-1$, and conditioning on $\mathbf{w} \sim q(\mathbf{w})$ and $\tilde{f} \sim q(\tilde{f})$, we utilize the state transition in Eq. (20) to perform the prediction step. This generates N predicted samples $\{\bar{\mathbf{x}}_t^{(i)}\}_{i=1}^N$ as follows:

$$\bar{\mathbf{x}}_t^{(i)} \sim \mathcal{N}(\mathbf{x}_t | \alpha_t \cdot \tilde{f}(\mathbf{x}_{t-1}^{(i)}) + \beta_t, \mathbf{Q}), i = 1, 2, \dots, N. \quad (28)$$

Therefore, the prediction distribution in Eq. (27) is approximated as:

$$p(\mathbf{x}_t | \mathbf{w}, \tilde{f}, \mathbf{y}_{1:t-1}) \approx \mathcal{N}(\mathbf{x}_t | \bar{\mathbf{m}}_t, \bar{\mathbf{P}}_t), \quad (29)$$

where

$$\bar{\mathbf{m}}_t = \frac{1}{N} \sum_{i=1}^N \bar{\mathbf{x}}_t^{(i)}, \quad (30a)$$

$$\bar{\mathbf{P}}_t = \frac{1}{N-1} \sum_{i=1}^N (\bar{\mathbf{x}}_t^{(i)} - \bar{\mathbf{m}}_t) (\bar{\mathbf{x}}_t^{(i)} - \bar{\mathbf{m}}_t)^\top. \quad (30b)$$

2) **Update:** Observations \mathbf{y}_t are then assimilated into the predictive ensemble to update the state estimate. Specifically, the predictive ensemble is updated using:

$$\text{update: } \mathbf{x}_t^{(i)} = \bar{\mathbf{x}}_t^{(i)} + \mathbf{G}_t(\mathbf{y}_t + \mathbf{e}_t^{(i)} - \mathbf{C}\bar{\mathbf{x}}_t^{(i)}), \quad (31a)$$

$$\text{reparameterization: } \mathbf{e}_t^{(i)} = \mathbf{0} + \mathbf{R}^{\frac{1}{2}}\epsilon, \epsilon \sim \mathcal{N}(\mathbf{0}, \mathbf{I}_{d_y}), \quad (31b)$$

Algorithm 1 ETGPSSM

Input: $\vartheta = \{\theta_{gp}, \psi, \mathbf{Q}, \mathbf{R}\}$, ζ , $\mathbf{y}_{1:T}$, $\mathbf{x}_0^{1:N} \sim q(\mathbf{x}_0)$

- 1: **while** iterations not terminated **do**
- 2: $\mathbf{w} \sim q(\mathbf{w})$, $L_\ell = 0$
- 3: **for** $t = 1, 2, \dots, T$ **do**
- 4: Get \tilde{f} from $q(\tilde{f})$ using Eq. (8) with $\mathbf{x}_* = \mathbf{x}_{t-1}$
- 5: Get prediction samples using Eq. (28)
- 6: Get empirical moments $\bar{\mathbf{m}}_t, \bar{\mathbf{P}}_t$ using Eq. (30)
- 7: Get Kalman gain: $\bar{\mathbf{G}}_t = \bar{\mathbf{P}}_t \mathbf{C}^\top (\mathbf{C} \bar{\mathbf{P}}_t \mathbf{C}^\top + \mathbf{R})^{-1}$
- 8: Get updated samples using Eq. (31)
- 9: Evaluate the log-likelihood using Eq. (33), and
- $L_\ell = L_\ell + \log p(\mathbf{y}_t | \mathbf{y}_{1:t-1}, \mathbf{w}, \tilde{f})$
- 10: **end for**
- 11: Evaluate \mathcal{L} based on L_ℓ and Eq. (25)
- 12: Maximize \mathcal{L} and update ϑ, ζ using Adam [52]
- 13: **end while**

Output: EnKF particles $\{\mathbf{x}_{0:T}^{(i)}\}_{i=1}^N$, model parameters ϑ , and variational parameters ζ .

where \mathbf{G}_t is the Kalman gain matrix given by:

$$\mathbf{G}_t = \bar{\mathbf{P}}_t \mathbf{C}^\top (\mathbf{C} \bar{\mathbf{P}}_t \mathbf{C}^\top + \mathbf{R})^{-1}. \quad (32)$$

Thus we can obtain the set of N updated samples $\{\mathbf{x}_t^{(i)}\}_{i=1}^N$ from the filtering distribution at time step t . These updated samples allow us to recursively compute the samples and prediction distribution for subsequent time steps.

Remark 2. The prediction and update steps are inherently differentiable, as the sampled latent states become differentiable with respect to the state transition function $\tilde{f}(\cdot)$ and the noise covariances \mathbf{Q} and \mathbf{R} . This property allows for a straightforward gradient-based optimization (e.g. Adam [52] in Algorithm 1), facilitating a practical learning framework for parameter estimation and model tuning [50], [37].

Based on the outlined prediction and update steps, the likelihood $p(\mathbf{y}_t | \mathbf{y}_{1:t-1}, \mathbf{w}, \tilde{f})$ in Eq. (26) can be easily evaluated. Specifically, at each time step t , we have:

$$p(\mathbf{y}_t | \mathbf{y}_{1:t-1}, \mathbf{w}, \tilde{f}) \approx \mathcal{N}(\mathbf{y}_t | \mathbf{C} \bar{\mathbf{m}}_t, \mathbf{C} \bar{\mathbf{P}}_t \mathbf{C}^\top), \quad (33)$$

due to the Gaussian prediction distribution, see Eq. (29), and the linear emission model, see Eq. (16e).

Now, we can evaluate our variational lower bound, \mathcal{L} , as defined in Eq. (25). At each step, we first utilize the reparameterization trick (see e.g. Eq. (31b)) to sample from the Gaussian variational distributions $q(\mathbf{w})$ and $q(\tilde{f})$. This allows us to obtain an unbiased estimate of the expected log-likelihood, $\mathbb{E}_{q(\mathbf{w}, \tilde{f})} [\log p(\mathbf{y}_t | \mathbf{y}_{1:t-1}, \mathbf{w}, \tilde{f})]$ numerically. Due to the reparameterization trick [53], \mathcal{L} is differentiable with respect to the model parameters $\vartheta = \{\theta_{gp}, \psi, \mathbf{Q}, \mathbf{R}\}$ and the variational parameters $\zeta = \{\mathbf{m}_0, \mathbf{L}_0, \mathbf{m}_w, \sigma_w^2, \mathbf{m}, \mathbf{S}, \bar{\mathbf{z}}\}$. Consequently, we leverage modern differentiation tools, such as PyTorch, to automatically compute the gradients through backpropagation through time (BPTT) and apply gradient-based optimization methods (e.g., Adam) to maximize \mathcal{L} [54], [52]. The detailed routine for implementing our EnKF-aided

ETGPSSM is summarized in Algorithm 1.

Remark 3 (Efficiency). *The proposed ETGPSSM in Algorithm 1 improves upon existing GPSSMs in two primary aspects of efficiency. First, its computational complexity is reduced from $\mathcal{O}(d_x M^3)$ to $\mathcal{O}(M^3)$ by utilizing a single GP—while the shallow neural network adds minimal computational overhead. Second, the use of a single GP and shallow neural network prevents the quadratic growth of variational parameters, as discussed in Section II-C. Moreover, by avoiding explicit parameterization of the latent states and instead leveraging the EnKF, the proposed method further reduces parametric complexity. Together, these design choices contribute to both parameterization and computational efficiency. Further empirical validation of these improvements is provided in Section IV-B.*

In the next section, we empirically evaluate the performance of ETGPSSM across various datasets.

IV. EXPERIMENTS

We first demonstrate the advantages of ETGPSSM in learning non-stationary dynamical systems in Section IV-A. Next, in Section IV-B, we highlight the computational and parametric efficiency and filtering performance of ETGPSSM in chaotic high-dimensional dynamical systems. Finally, Section IV-C showcases the superior prediction performance of ETGPSSM using multiple real-world time series datasets. More experimental details can be found in the accompanying source code, which is publicly available online.⁴

A. Non-Stationary Dynamical System Learning

This subsection demonstrates the superior modeling capabilities of ETGPSSM over existing GPSSM and neural network-based methods by evaluating the learning performance on the following underlying dynamical system:

$$\mathbf{x}_{t+1} = f(\mathbf{x}_t) + \mathbf{v}_t, \quad \mathbf{v}_t \sim \mathcal{N}(0, \sigma_Q^2), \quad (34a)$$

$$\mathbf{y}_t = \mathbf{x}_t + \mathbf{e}_t, \quad \mathbf{e}_t \sim \mathcal{N}(0, \sigma_R^2), \quad (34b)$$

where the *non-stationary kink function* $f(\mathbf{x})$ is defined as:

$$f(\mathbf{x}) = \underbrace{\left[0.8 + (\mathbf{x} + 0.2) \left(1 - \frac{5}{1 + \exp(-2\mathbf{x})} \right) \right]}_{\text{"kink" function}} s(\mathbf{x}) - o(\mathbf{x}) \quad (35)$$

with a slope function:

$$s(\mathbf{x}) = \begin{cases} 1 - 0.5 \exp(-0.5\mathbf{x}), & \mathbf{x} > 0, \\ 1, & \mathbf{x} \leq 0, \end{cases} \quad (36)$$

and an oscillatory function:

$$o(\mathbf{x}) = \begin{cases} 0.5 \sin(8\mathbf{x}), & \mathbf{x} > 0, \\ 0.5 \sin(2\mathbf{x}), & \mathbf{x} \leq 0. \end{cases} \quad (37)$$

The slope and oscillatory functions create non-stationary pattern across different regions of the “kink” function (see Fig. 4).

Using this underlying SSM, we generate training data $\mathbf{y}_{1:T}$ by fixing σ_Q^2 at 0.05 and varying σ_R^2 systematically

across the set $\{0.0008, 0.008, 0.08, 0.8\}$, resulting in four sets of $T = 600$ observations each for training purposes. To demonstrate the advantages of ETGPSSM, we compare it with the state-of-the-art (SOTA) neural network-based AD-EnKFs [50] and GP-based EnVI [37]. Consistent with previous works [31], [37], we retain the true emission model and allow the transition model to be learned in all methods, ensuring a fair comparison within the latent space. The system dynamics learning results across different methods are shown in Fig. 4, where our method is represented in the last two columns. The suffixes “DNN” and “BNN” in brackets indicate the network types—Bayesian neural network (BNN) or deep neural network (DNN)—used in our model (see Fig. 3).

The results in Fig. 4 demonstrate that ETGPSSMs consistently achieve superior system dynamics learning performance. Under small observational noise levels ($\sigma_R^2 = \{0.0008, 0.008\}$), ETGPSSMs—particularly ETGPSSM with DNN—excel in learning the dynamics of non-stationary systems. In contrast, their competitor, AD-EnKFs, fails to capture the smooth left segment of the kink function and performs well only on the more zigzag right segment. Meanwhile, EnVI, the SOTA GPSSM, fails to capture the non-stationary behavior of the system and is unable to model the zigzag region effectively. These results highlight the strength of ETGPSSMs in integrating the representational flexibility of neural networks with the GPs, making them particularly well-suited for modeling non-stationary dynamics.

When the observational noise interference becomes more significant ($\sigma_R^2 = \{0.08, 0.8\}$), the learning performance of all methods deteriorates. This is due to the higher estimation errors in the latent states, which hinder accurate learning of the system dynamics. Nevertheless, ETGPSSMs continue to demonstrate superior learning performance. Notably, in this scenario, BNN-based methods, particularly ETGPSSM (BNN), exhibit superior performance and more reliable uncertainty quantification compared to their DNN-based counterparts. These results highlight not only the effectiveness of ETGPSSM’s non-stationary modeling capabilities but also the regularization benefits inherent in Bayesian methods, which contribute to enhanced robustness against significant observational noise.

B. High-Dimensional Latent State Estimation

In this subsection, we focus on latent state estimation in the Lorenz-96 system, a mathematical model for studying chaotic behavior in weather and climate dynamics [55]. The system consists of $d_x \in \mathbb{Z}_+$ coupled ordinary differential equations (ODEs):

$$\frac{dx_{t,d}}{dt} = (x_{t,d+1} - x_{t,d-2})x_{t,d-1} - x_{t,d} + F, \quad 1 \leq d \leq d_x. \quad (38)$$

Here the constant forcing parameter F is set to 8, resulting in a fully chaotic dynamic [55], where small variations in initial conditions lead to vastly different trajectories. The dynamics model is discretized using the Euler method, and at each time step t , observations are generated through a linear emission model ($\mathbf{C} = \mathbf{I}$) with Gaussian additive noise, where the noise level is significant with the covariance given by $\mathbf{R} = 4\mathbf{I}$.

⁴https://github.com/zhidilin/gpssmProj/tree/main/high_dim_GPSSM

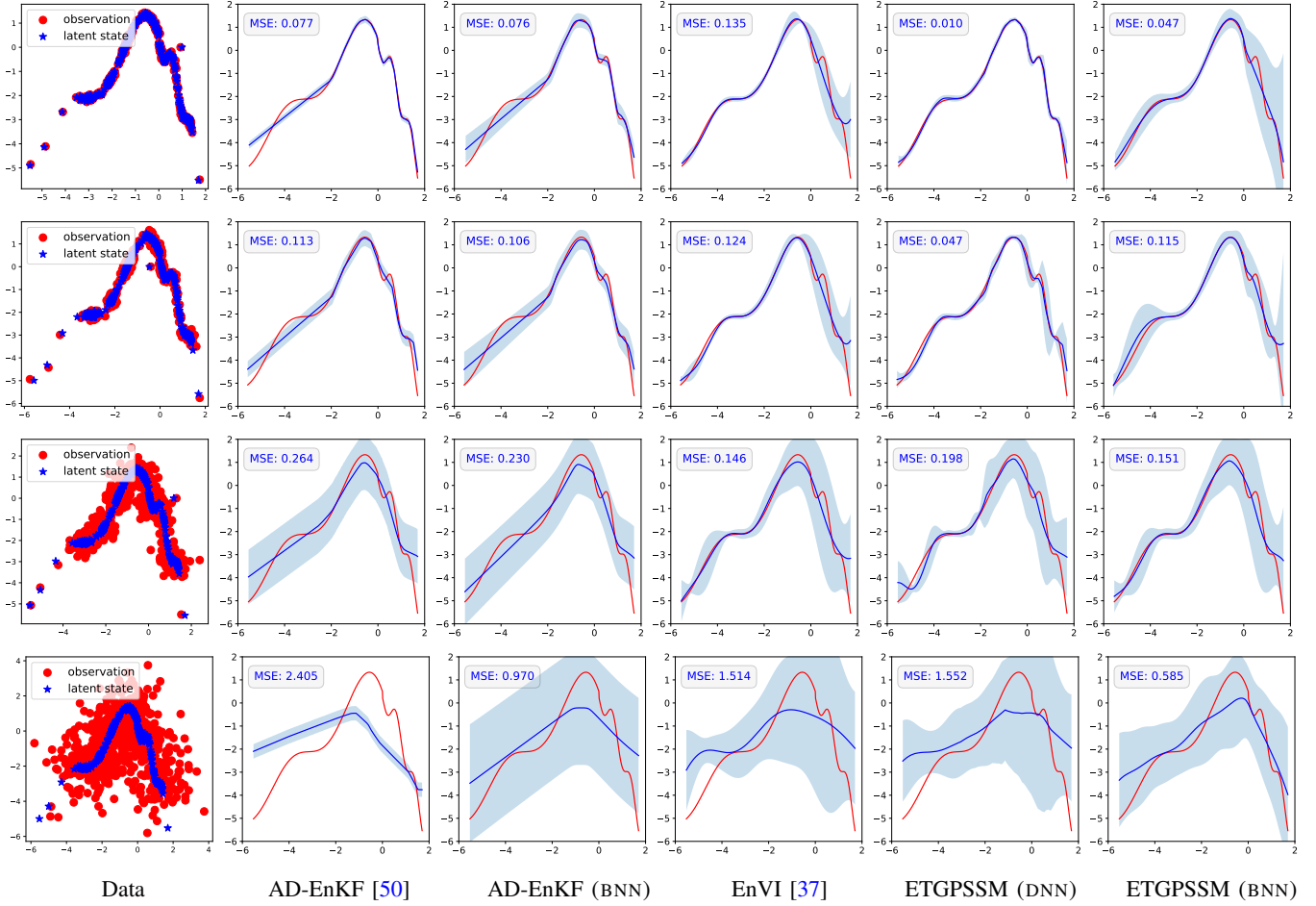


Fig. 4: Non-stationary *kink* transition function learning performance (mean $\pm 2\sigma$) using various methods across different levels of emission noise ($\sigma_R^2 \in \{0.0008, 0.008, 0.08, 0.8\}$, from top to bottom). The blue curve (---) represents the learned mean function, while the red line (---) indicates the true system transition function. The shaded blue region depicts the confidence interval.

We first empirically demonstrate the efficiency of ETGPSSM in high-dimensional latent state spaces, as illustrated in Fig. 5. This figure highlights both the computational efficiency and the parameter scalability of ETGPSSM in comparison to conventional GPSSMs across varying latent dimensions. The shallow neural network used in ETGPSSM is a three-layer fully connected architecture with ReLU activation and hidden dimensions of 128 and 64, which maps from \mathbb{R}^{d_x} to the flow parameter space $\Theta \subseteq \mathbb{R}^{2d_x}$. As shown in the left panel, the number of parameters in ETGPSSM increases linearly with the latent state dimension d_x , in contrast to the quadratic parameter growth observed in GPSSMs. This linear scalability is achieved through the use of a single shared GP combined with normalizing flows, which drastically reduces the total number of parameters compared to GPSSMs that rely on independent GPs for each state dimension.

The right panel of Fig. 5 illustrates the computational efficiency of ETGPSSM by comparing the one-sample execution time for transition evaluation (i.e., Eq. (1a)). Notably, ETGPSSM maintains consistently low running times across increasing state dimensions, whereas GPSSM exhibits rapid growth in computational cost. For instance, at $d_x = 100$, ETG-

PSSM completes the evaluation in 0.36 seconds, significantly outperforming GPSSM, which requires 19.56 seconds. This efficiency stems from the reduced computational complexity of ETGPSSM, which scales as $\mathcal{O}(M^3)$ due to its use of a single GP, in contrast to GPSSM’s $\mathcal{O}(d_x M^3)$ complexity. These results demonstrate that ETGPSSM achieves more scalable parameter growth with increasing state dimensionality while maintaining computational tractability in high-dimensional settings, making it a practical choice for modeling high-dimensional chaotic systems like the Lorenz-96 system.

We next fix the dimension $d_x = 100$ in the Lorenz-96 system and generate observations of length $T = 600$ for training ETGPSSM and its deep neural network-based competitor, AD-EnKF [50]. The EnVI [37], which already caused out-of-memory errors⁵ at $d_x = 30$ with an ensemble size $N = 150$, is excluded due to its prohibitive computational cost in this high-dimensional setting. The corresponding state inference performance after training is shown in Fig. 6, where the

⁵All experiments were conducted on a machine equipped with an Intel Xeon W7-3545 v6 processor (24 cores, 2.7 GHz), 128 GB of DDR5 RAM, and an NVIDIA RTX 4500 Ada GPU (24 GB VRAM), running Ubuntu 20.04 LTS.

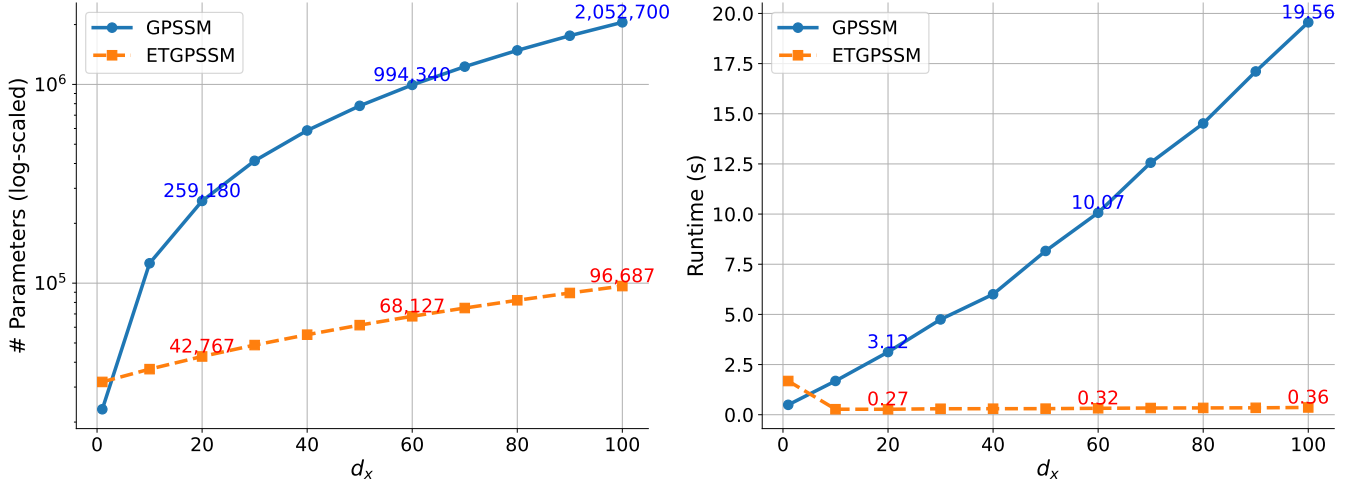


Fig. 5: **(Left)** The number of parameters in ETGPSSM grows linearly with the state dimension d_x , whereas in GPSSM, it scales quadratically. **(Right)** ETGPSSM maintains low computational costs as d_x increases, while GPSSM exhibits linear growth.

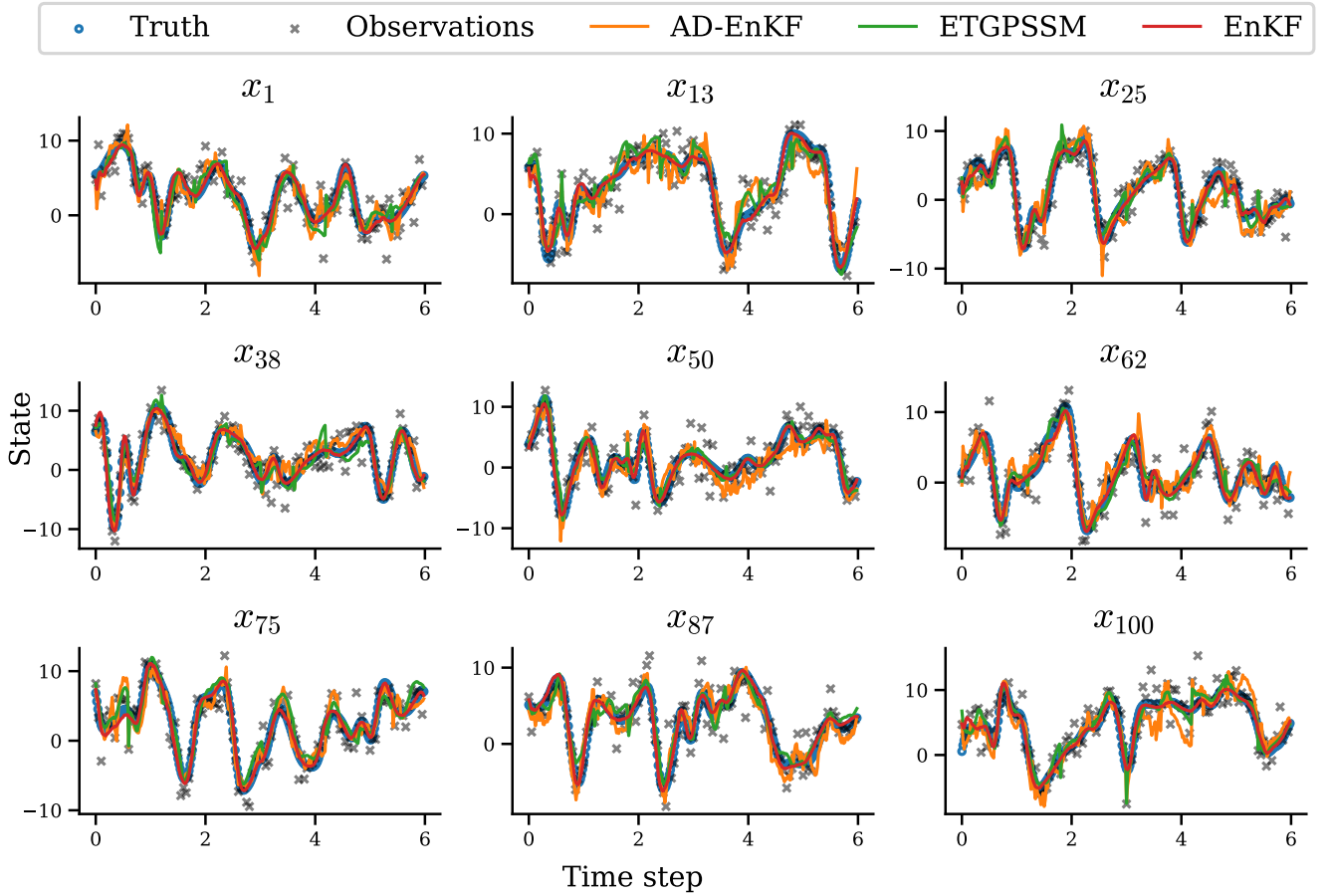


Fig. 6: Latent state estimation performance for 100-dimensional Lorenz-96 system, with 9 dimensions uniformly sampled for visualization. Root mean square error (RMSE) values for different methods: 0.5468 for EnKF, 1.2028 for ETGPSSM, 1.6187 for AD-EnKF. RMSE between latent states and observations: 1.9855.

performance of EnKF is also included for comparison.

As illustrated in Fig. 6, ETGPSSM achieves a root mean square error (RMSE) of 1.2028, outperforming AD-EnKF, which yields an RMSE of 1.6187. This result highlights the superior filtering performance of ETGPSSM in high-dimensional

chaotic systems. Additionally, the RMSE of the observations (1.9855) serves as a baseline, demonstrating that ETGPSSM significantly reduces the estimation error compared to the raw observations. Although EnKF yields the lowest RMSE of 0.5468, it relies on full model knowledge and does not

TABLE I: Prediction performance in terms of RMSE of the different models on the system identification datasets. Mean and standard deviation of the prediction results are shown as an averaged result over ten different seeds. The three lowest RMSE values are highlighted in shades of green, with a deeper one indicating lower RMSE.

Method	Actuator	Ball Beam	Drive	Dryer	Gas Furnace
DKF [7]	1.204 \pm 0.250	0.144 \pm 0.005	0.735 \pm 0.001	1.465 \pm 0.087	5.589 \pm 0.066
AD-EnKF [50]	0.705 \pm 0.117	0.057 \pm 0.006	0.756 \pm 0.114	0.182 \pm 0.053	1.408 \pm 0.090
AD-EnKF (BNN)	0.705 \pm 0.088	0.053 \pm 0.007	0.896 \pm 0.088	0.155 \pm 0.030	1.361 \pm 0.061
vGPSSM [29]	1.640 \pm 0.011	0.268 \pm 0.414	0.740 \pm 0.010	0.822 \pm 0.002	3.676 \pm 0.145
CO-GPSSM [36]	0.803 \pm 0.011	0.079 \pm 0.018	0.736 \pm 0.007	0.366 \pm 0.146	1.898 \pm 0.157
PRSSM [30]	0.691 \pm 0.148	0.074 \pm 0.010	0.647 \pm 0.057	0.174 \pm 0.013	1.503 \pm 0.196
ODGPSSM [39]	0.666 \pm 0.074	0.068 \pm 0.006	0.708 \pm 0.052	0.171 \pm 0.011	1.704 \pm 0.560
VCDT [31]	0.815 \pm 0.012	0.065 \pm 0.005	0.735 \pm 0.005	0.667 \pm 0.266	2.052 \pm 0.163
EnVI [37]	0.657 \pm 0.095	0.055 \pm 0.002	0.703 \pm 0.050	0.125 \pm 0.017	1.388 \pm 0.123
ETGPSSM (DNN)	0.646 \pm 0.081	0.050 \pm 0.003	0.668 \pm 0.092	0.137 \pm 0.030	1.300 \pm 0.052
ETGPSSM (BNN)	0.646 \pm 0.095	0.053 \pm 0.002	0.703 \pm 0.028	0.154 \pm 0.026	1.313 \pm 0.048

learn system dynamics. In contrast, ETGPSSM simultaneously learns dynamics and infers latent states, offering a more versatile and effective solution for high-dimensional complex systems.

C. Real-World Time Series Prediction

In this subsection, we evaluate the prediction performance of ETGPSSM on several real-world time series datasets commonly used for system identification (see Table I). The prediction RMSE results are summarized in Table I, comparing ETGPSSM against SOTA methods, including neural network-based approaches—DKF [7] and AD-EnKF [50]—as well as various GPSSMs: vGPSSM [29], CO-GPSSM [36], PRSSM [30], ODGPSSM [39], VCDT [31], and EnVI [37]. Following previous works, the latent space dimension is set to $d_x = 4$ for all the methods.

As shown in Table I, ETGPSSM demonstrates competitive performance across all datasets. Notably, on the *Actuator* dataset, ETGPSSM (DNN) and ETGPSSM (BNN) both achieve an improved RMSE of 0.646, outperforming EnVI (0.657) and significantly improving upon AD-EnKFs, which record an RMSE of 0.705. Similarly, on the *Ball Beam* and *Gas Furnace* datasets, ETGPSSMs attain the first and second lowest RMSEs, highlighting their ability to accurately model system dynamics. However, on datasets such as *Drive* and *Dryer*, other GPSSMs like PRSSM and EnVI achieve slightly superior performance. This can be attributed to the relatively low latent state dimension ($d_x = 4$), where traditional GPSSMs, such as PRSSM, ODGPSSM and EnVI, remain highly competitive, as discussed in [37]. Nonetheless, we emphasize that the proposed ETGPSSM remains highly competitive, achieving very comparable performance even in low-dimensional settings, while significantly reducing computational complexity and parameter overhead—thereby ensuring both scalability and efficiency in high-dimensional scenarios.

In comparison to neural network-based methods like AD-EnKF, the superior performance of ETGPSSM is driven by its ability to integrate the strengths of GPs and neural networks.

This hybrid approach allows ETGPSSM to effectively model complex, non-stationary system dynamics while providing reliable predictions—an area where pure deep neural network-based methods often struggle. This is evident from the results, where neural network-based methods exhibit higher prediction errors. Notably, AD-EnKF (BNN) generally outperforms other network-based approaches, corroborating the benefits of Bayesian treatments, particularly their inherent regularization, which helps mitigate overfitting and improve generalization. In summary, the experimental results demonstrate that ETGPSSM is a powerful and versatile tool for real-world time series prediction.

V. CONCLUSIONS

In this paper, we presented a novel approach for learning and inference in GPSSMs tailored to non-stationary, high-dimensional dynamical systems. Our key contribution is the introduction of the ETGP prior, which integrates a shared GP with input-dependent normalizing flows modeled via neural networks. This ETGP enhances flexibility in capturing complex, non-stationary transitions while significantly reducing the computational and parametric complexity of traditional GPSSMs in high-dimensional settings. To enable scalable inference, we developed a variational framework that approximates the posterior over the ETGP by separately modeling the underlying GP and neural network parameters. Additionally, we leverage the EnKF to circumvent the need for explicit parameterization of state posteriors, further improving computational efficiency. Empirical evaluations across dynamical system learning, high-dimensional state estimation, and time-series prediction tasks demonstrate that our method outperforms existing GPSSMs and deep neural network-based SSMs, while maintaining lower computational and parametric complexity.

APPENDIX A

PROOF OF COROLLARY 1

Proof. Similar proof of this corollary has been discussed in the literature; see [48]. For ease of reference, we also detail

here. Consider two arbitrary time steps t and t' , we have

$$\mathbf{f}(\mathbf{x}_{t-1}) = \boldsymbol{\alpha}_t \cdot \tilde{\mathbf{f}}(\mathbf{x}_{t-1}) + \boldsymbol{\beta}_t, \quad (39)$$

$$\mathbf{f}(\mathbf{x}_{t'-1}) = \boldsymbol{\alpha}_{t'} \cdot \tilde{\mathbf{f}}(\mathbf{x}_{t'-1}) + \boldsymbol{\beta}_{t'}. \quad (40)$$

Since $\boldsymbol{\theta}_t$ and $\boldsymbol{\theta}_{t'}$ are deterministic, the joint distribution of $\mathbf{f}(\mathbf{x}_{t-1})$ and $\mathbf{f}(\mathbf{x}_{t'-1})$ is Gaussian with mean $[\boldsymbol{\beta}_t^\top, \boldsymbol{\beta}_{t'}^\top]^\top$.

The covariance between $\mathbf{f}(\mathbf{x}_{t-1})$ and $\mathbf{f}(\mathbf{x}_{t'-1})$ is:

$$\boldsymbol{\Lambda}_{t,t'} = \boldsymbol{\alpha}_t \cdot \text{Cov}(\tilde{\mathbf{f}}(\mathbf{x}_{t-1}), \tilde{\mathbf{f}}(\mathbf{x}_{t'-1})) \cdot \boldsymbol{\alpha}_{t'}^\top \quad (41)$$

$$= k(\mathbf{x}_{t-1}, \mathbf{x}_{t'-1}) \cdot \boldsymbol{\alpha}_t \boldsymbol{\alpha}_{t'}^\top. \quad (42)$$

Similarly, the covariance of $\mathbf{f}(\mathbf{x}_{t-1})$ with itself is:

$$\text{Cov}(\mathbf{f}(\mathbf{x}_{t-1}), \mathbf{f}(\mathbf{x}_{t-1})) = k(\mathbf{x}_{t-1}, \mathbf{x}_{t-1}) \cdot \boldsymbol{\alpha}_t \boldsymbol{\alpha}_t^\top. \quad (43)$$

The same logic applies to $\mathbf{f}(\mathbf{x}_{t'-1})$. Therefore, the covariance matrix $\boldsymbol{\Lambda}_{t,t'}$ is:

$$\boldsymbol{\Lambda}_{t,t'} = \begin{bmatrix} k(\mathbf{x}_{t-1}, \mathbf{x}_{t-1}) \cdot \boldsymbol{\alpha}_t \boldsymbol{\alpha}_t^\top & k(\mathbf{x}_{t-1}, \mathbf{x}_{t'-1}) \cdot \boldsymbol{\alpha}_t \boldsymbol{\alpha}_{t'}^\top \\ k(\mathbf{x}_{t'-1}, \mathbf{x}_{t-1}) \cdot \boldsymbol{\alpha}_{t'} \boldsymbol{\alpha}_t^\top & k(\mathbf{x}_{t'-1}, \mathbf{x}_{t'-1}) \cdot \boldsymbol{\alpha}_{t'} \boldsymbol{\alpha}_{t'}^\top \end{bmatrix}. \quad (44)$$

□

APPENDIX B

ELBO DERIVATIONS AND APPROXIMATIONS

Given the joint distribution of our model in Eq. (18) and the variational distribution in Eq. (21), augmented by the sparse GP, we can formulate the ELBO according to the general definition provided in Eq. (17). The detailed derivations are presented in Eq. (45).

From Eq. (45d) to Eq. (45e), we have made the following two assumptions, similar to the work in [37]:

- 1) $p(\mathbf{x}_{t-1} | \mathbf{w}, \tilde{\mathbf{f}}, \mathbf{y}_{1:t-1}) \approx p(\mathbf{x}_{t-1} | \mathbf{w}, \tilde{\mathbf{f}}, \mathbf{y}_{1:t})$,
- 2) $q(\mathbf{x}_t | \mathbf{w}, \tilde{\mathbf{f}}, \mathbf{x}_{t-1}) \approx p(\mathbf{x}_t | \mathbf{w}, \tilde{\mathbf{f}}, \mathbf{x}_{t-1}, \mathbf{y}_{1:t})$.

The transition from Eq. (45f) to Eq. (45g) is derived straightforwardly by applying Bayes' theorem.

The two approximations used here are similar to those in [37], with the key difference being the focus on the ETGP in this paper rather than the GP. The rationale behind these approximations is as follows:

- Assumption 1) assumes that the posterior distribution of the latent state at time $t-1$ based on observations up to $t-1$ is nearly identical to that based on observations up to t . This holds particularly well when t is large, as the additional observation at time t has minimal impact on the state estimate due to the accumulated information over time.
- Assumption 2) posits that the variational distribution $q(\mathbf{x}_t | \mathbf{w}, \tilde{\mathbf{f}}, \mathbf{x}_{t-1})$ is approximated by the filtering distribution $p(\mathbf{x}_t | \mathbf{w}, \tilde{\mathbf{f}}, \mathbf{x}_{t-1}, \mathbf{y}_{1:t})$. Note that in variational inference, the variational distribution serves as an approximation of the true smoothing distribution $p(\mathbf{x}_t | \mathbf{w}, \tilde{\mathbf{f}}, \mathbf{x}_{t-1}, \mathbf{y}_{1:T})$. While there may be some estimation loss, the approximation is reasonable for long observation sequences where future observations minimally affect state estimates. This trade-off balances accuracy and computational efficiency, a crucial consideration in high-dimensional settings.

REFERENCES

- [1] S. Särkkä and L. Svensson, *Bayesian filtering and smoothing*. Cambridge university press, 2023, vol. 17.
- [2] A. Kullberg, I. Skog, and G. Hendeby, "Online joint state inference and learning of partially unknown state-space models," *IEEE Trans. Signal Process.*, vol. 69, pp. 4149–4161, 2021.
- [3] U. A. Khan and J. M. Moura, "Distributing the Kalman filter for large-scale systems," *IEEE Trans. Signal Process.*, vol. 56, no. 10, pp. 4919–4935, 2008.
- [4] F. Tobar, P. M. Djurić, and D. P. Mandic, "Unsupervised state-space modeling using reproducing kernels," *IEEE Trans. Signal Process.*, vol. 63, no. 19, pp. 5210–5221, 2015.
- [5] G. Revach, N. Shlezinger, X. Ni, A. L. Escoriza, R. J. Van Sloun, and Y. C. Eldar, "KalmanNet: Neural network aided Kalman filtering for partially known dynamics," *IEEE Trans. Signal Process.*, vol. 70, pp. 1532–1547, 2022.
- [6] L. Girin, S. Leglaive, X. Bie, J. Diard, T. Hueber, and X. Alameda-Pineda, "Dynamical variational autoencoders: A comprehensive review," *Found. Trends Mach. Learn.*, vol. 15, no. 1–2, pp. 1–175, 2021.
- [7] R. Krishnan, U. Shalit, and D. Sontag, "Structured inference networks for nonlinear state space models," in *Proc. AAAI Conf. Artif. Intell. (AAAI)*, 2017, pp. 2101–2109.
- [8] A. Ghosh, A. Honoré, and S. Chatterjee, "DANSE: Data-driven nonlinear state estimation of model-free process in unsupervised learning setup," *IEEE Trans. Signal Process.*, pp. 1824–1838, 2024.
- [9] C. E. Rasmussen and C. K. I. Williams, *Gaussian Processes for Machine Learning*. MIT Press, 2006.
- [10] R. Frigola, "Bayesian time series learning with Gaussian processes," Ph.D. dissertation, University of Cambridge, 2015.
- [11] R. C. Suwandi, Z. Lin, F. Yin, Z. Wang, and S. Theodoridis, "Sparsity-aware distributed learning for Gaussian processes with linear multiple kernel," *IEEE Trans. Neural Netw. Learn. Syst.*, pp. 1–15, Jan. 2025.
- [12] J. M. Wang, D. J. Fleet, and A. Hertzmann, "Gaussian process dynamical models for human motion," *IEEE Trans. Pattern Anal. Mach. Intell.*, vol. 30, no. 2, pp. 283–298, 2007.
- [13] M. P. Deisenroth, D. Fox, and C. E. Rasmussen, "Gaussian processes for data-efficient learning in robotics and control," *IEEE Trans. Pattern Anal. Mach. Intell.*, vol. 37, no. 2, pp. 408–423, 2013.
- [14] K. Arulkumaran, M. P. Deisenroth, M. Brundage, and A. A. Bharath, "Deep reinforcement learning: A brief survey," *IEEE Signal Process. Mag.*, vol. 34, no. 6, pp. 26–38, 2017.
- [15] Z. Yan, P. Cheng, Z. Chen, Y. Li, and B. Vucetic, "Gaussian process reinforcement learning for fast opportunistic spectrum access," *IEEE Trans. Signal Process.*, vol. 68, pp. 2613–2628, 2020.
- [16] A. Xie, F. Yin, B. Ai, S. Zhang, and S. Cui, "Learning while tracking: A practical system based on variational Gaussian process state-space model and smartphone sensory data," in *Proc. Int. Conf. Inf. Fusion (FUSION)*, 2020, pp. 1–7.
- [17] K. Berntorp and M. Menner, "Constrained Gaussian-process state-space models for online magnetic-field estimation," in *Proc. Int. Conf. Inf. Fusion (FUSION)*, 2023, pp. 1–7.
- [18] J. Ko and D. Fox, "GP-BayesFilters: Bayesian filtering using Gaussian process prediction and observation models," *Auton. Robots*, vol. 27, no. 1, pp. 75–90, 2009.
- [19] M. P. Deisenroth, M. F. Huber, and U. D. Hanebeck, "Analytic moment-based Gaussian process filtering," in *Proc. Int. Conf. Mach. Learn. (ICML)*, 2009, pp. 225–232.
- [20] M. P. Deisenroth, R. D. Turner, M. F. Huber, U. D. Hanebeck, and C. E. Rasmussen, "Robust filtering and smoothing with Gaussian processes," *IEEE Trans. Autom. Control*, vol. 57, no. 7, pp. 1865–1871, 2011.
- [21] J. Ko and D. Fox, "Learning GP-BayesFilters via Gaussian process latent variable models," *Auton. Robots*, vol. 30, no. 1, pp. 3–23, 2011.
- [22] R. Frigola, F. Lindsten, T. B. Schön, and C. E. Rasmussen, "Bayesian inference and learning in Gaussian process state-space models with particle MCMC," in *Proc. Adv. Neural Inf. Process. Syst. (NeurIPS)*, 2013, pp. 3156–3164.
- [23] A. Svensson, A. Solin, S. Särkkä, and T. Schön, "Computationally efficient Bayesian learning of Gaussian process state space models," in *Proc. Int. Conf. Artif. Intell. Stat. (AISTATS)*, 2016, pp. 213–221.
- [24] A. Svensson and T. B. Schön, "A flexible state-space model for learning nonlinear dynamical systems," *Automatica*, vol. 80, pp. 189–199, 2017.
- [25] K. Berntorp, "Online Bayesian inference and learning of Gaussian-process state-space models," *Automatica*, vol. 129, p. 109613, 2021.
- [26] Y. Liu, M. Ajirak, and P. M. Djurić, "Sequential estimation of Gaussian process-based deep state-space models," *IEEE Trans. Signal Process.*, vol. 71, pp. 2968–2980, 2023.

$$\mathcal{L} = \mathbb{E}_q \left[\log \frac{p(\tilde{\mathbf{y}}, \tilde{\mathbf{x}}, \mathbf{w}, \tilde{f}, \mathbf{u})}{q(\tilde{\mathbf{x}}, \mathbf{w}, \tilde{f}, \mathbf{u})} \right] \quad (45a)$$

$$= \mathbb{E}_q \left[\log \frac{p(\tilde{f}, \mathbf{u}) p(\mathbf{w}) p(\mathbf{x}_0) \prod_{t=1}^T p(\mathbf{y}_t | \mathbf{x}_t) p(\mathbf{x}_t | \mathbf{w}, \tilde{f}, \mathbf{x}_{t-1})}{q(\tilde{f}, \mathbf{u}) q(\mathbf{w}) q(\mathbf{x}_0) \prod_{t=1}^T q(\mathbf{x}_t | \mathbf{w}, \tilde{f}, \mathbf{x}_{t-1})} \right] \quad (45b)$$

$$= \mathbb{E}_q \left[\sum_{t=1}^T \log \frac{p(\mathbf{y}_t, \mathbf{x}_t | \mathbf{w}, \tilde{f}, \mathbf{x}_{t-1})}{q(\mathbf{x}_t | \mathbf{w}, \tilde{f}, \mathbf{x}_{t-1})} \right] - \text{KL}(q(\mathbf{u}) \| p(\mathbf{u})) - \text{KL}(q(\mathbf{w}) \| p(\mathbf{w})) - \text{KL}(q(\mathbf{x}_0) \| p(\mathbf{x}_0)) \quad (45c)$$

$$= \mathbb{E}_q \left[\sum_{t=1}^T \log \frac{p(\mathbf{y}_t, \mathbf{x}_t | \mathbf{w}, \tilde{f}, \mathbf{x}_{t-1}) p(\mathbf{x}_{t-1} | \mathbf{w}, \tilde{f}, \mathbf{y}_{1:t-1})}{q(\mathbf{x}_t | \mathbf{w}, \tilde{f}, \mathbf{x}_{t-1}) p(\mathbf{x}_{t-1} | \mathbf{w}, \tilde{f}, \mathbf{y}_{1:t-1})} \right] - \text{KL}(q(\mathbf{u}) \| p(\mathbf{u})) - \text{KL}(q(\mathbf{w}) \| p(\mathbf{w})) - \text{KL}(q(\mathbf{x}_0) \| p(\mathbf{x}_0)) \quad (45d)$$

$$\approx \mathbb{E}_q \left[\sum_{t=1}^T \log \frac{p(\mathbf{y}_t, \mathbf{x}_t | \mathbf{w}, \tilde{f}, \mathbf{x}_{t-1}) p(\mathbf{x}_{t-1} | \mathbf{w}, \tilde{f}, \mathbf{y}_{1:t-1})}{\underbrace{p(\mathbf{x}_t | \mathbf{w}, \tilde{f}, \mathbf{x}_{t-1})}_{\text{assumption 1}} \underbrace{p(\mathbf{x}_{t-1} | \mathbf{w}, \tilde{f}, \mathbf{y}_{1:t-1})}_{\text{assumption 2}}} \right] - \text{KL}(q(\mathbf{u}) \| p(\mathbf{u})) - \text{KL}(q(\mathbf{w}) \| p(\mathbf{w})) - \text{KL}(q(\mathbf{x}_0) \| p(\mathbf{x}_0)) \quad (45e)$$

$$= \mathbb{E}_q \left[\sum_{t=1}^T \log \frac{p(\mathbf{y}_t, \mathbf{x}_t, \mathbf{x}_{t-1} | \mathbf{w}, \tilde{f}, \mathbf{y}_{1:t-1})}{p(\mathbf{x}_t, \mathbf{x}_{t-1} | \mathbf{w}, \tilde{f}, \mathbf{y}_{1:t-1}, \mathbf{y}_t)} \right] - \text{KL}(q(\mathbf{u}) \| p(\mathbf{u})) - \text{KL}(q(\mathbf{w}) \| p(\mathbf{w})) - \text{KL}(q(\mathbf{x}_0) \| p(\mathbf{x}_0)) \quad (45f)$$

$$= \mathbb{E}_{q(\mathbf{w}, \tilde{f})} \left[\sum_{t=1}^T \log p(\mathbf{y}_t | \mathbf{y}_{1:t-1}, \mathbf{w}, \tilde{f}) \right] - \text{KL}(q(\mathbf{u}) \| p(\mathbf{u})) - \text{KL}(q(\mathbf{w}) \| p(\mathbf{w})) - \text{KL}(q(\mathbf{x}_0) \| p(\mathbf{x}_0)) \quad (45g)$$

-
- [27] R. Frigola, Y. Chen, and C. E. Rasmussen, “Variational Gaussian process state-space models,” in *Proc. Adv. Neural Inf. Process. Syst. (NeurIPS)*, 2014, pp. 3680–3688.
- [28] A. J. McHutchon, “Nonlinear modelling and control using Gaussian processes,” Ph.D. dissertation, University of Cambridge, 2014.
- [29] S. Eleftheriadis, T. Nicholson, M. P. Deisenroth, and J. Hensman, “Identification of Gaussian process state space models,” in *Proc. Adv. Neural Inf. Process. Syst. (NeurIPS)*, 2017, pp. 5309–5319.
- [30] A. Doerr, C. Daniel, M. Schiegg, N.-T. Duy, S. Schaal, M. Toussaint, and T. Sebastian, “Probabilistic recurrent state-space models,” in *Proc. Int. Conf. Mach. Learn. (ICML)*, 2018, pp. 1280–1289.
- [31] A. D. Ialongo, M. van der Wilk, J. Hensman, and C. E. Rasmussen, “Overcoming mean-field approximations in recurrent Gaussian process models,” in *Proc. Int. Conf. Mach. Learn. (ICML)*, 2019, pp. 2931–2940.
- [32] S. Curi, S. Melchior, F. Berkenkamp, and A. Krause, “Structured variational inference in partially observable unstable Gaussian process state space models,” in *Proc. Learning for Dynamics and Control (LADC)*, 2020, pp. 147–157.
- [33] Y. Liu and P. M. Djurić, “Gaussian process state-space models with time-varying parameters and inducing points,” in *Proc. European Signal Process. Conf. (EUSIPCO)*, 2021, pp. 1462–1466.
- [34] J. Lindinger, B. Rakitsch, and C. Lippert, “Laplace approximated Gaussian process state-space models,” in *Proc. Conf. Uncertain. Artif. Intell. (UAI)*, vol. 180, 2022, pp. 1199–1209.
- [35] X. Fan, E. V. Bonilla, T. O’Kane, and S. A. Sisson, “Free-form variational inference for Gaussian process state-space models,” in *Proc. Int. Conf. Mach. Learn. (ICML)*, 2023, pp. 9603–9622.
- [36] Z. Lin, F. Yin, and J. Maroñas, “Towards flexibility and interpretability of Gaussian process state-space model,” *arXiv preprint arXiv:2301.08843*, 2023.
- [37] Z. Lin, Y. Sun, F. Yin, and A. Thiéry, “Ensemble Kalman filtering meets Gaussian process SSM for non-mean-field and online inference,” *IEEE Trans. Signal Process.*, vol. 72, pp. 4286–4301, Aug. 2024.
- [38] Z. Lin, J. Maroñas, Y. Li, F. Yin, and S. Theodoridis, “Towards efficient modeling and inference in multi-dimensional Gaussian process state-space models,” in *Proc. IEEE Int. Conf. Acoust. Speech Signal Process. (ICASSP)*, 2024, pp. 12 881–12 885.
- [39] Z. Lin, L. Cheng, F. Yin, L. Xu, and S. Cui, “Output-dependent Gaussian process state-space model,” in *Proc. IEEE Int. Conf. Acoust. Speech Signal Process. (ICASSP)*, 2023, pp. 1–5.
- [40] M. Titsias, “Variational learning of inducing variables in sparse Gaussian processes,” in *Proc. Int. Conf. Artif. Intell. Stat. (AISTATS)*, 2009, pp. 567–574.
- [41] J. Hensman, N. Fusi, and N. D. Lawrence, “Gaussian processes for big data,” in *Proc. Conf. Uncertain. Artif. Intell. (UAI)*, 2013, pp. 282–290.
- [42] C. Ma, Y. Li, and J. M. Hernández-Lobato, “Variational implicit processes,” in *Proc. Int. Conf. Mach. Learn. (ICML)*, 2019, pp. 4222–4233.
- [43] I. Kobyzev, S. J. Prince, and M. A. Brubaker, “Normalizing flows: An introduction and review of current methods,” *IEEE Trans. Pattern Anal. Mach. Intell.*, vol. 43, no. 11, pp. 3964–3979, 2020.
- [44] J. Maroñas, O. Hamelijnck, J. Knoblauch, and T. Damoulas, “Transforming Gaussian processes with normalizing flows,” in *Proc. Int. Conf. Artif. Intell. Stat. (AISTATS)*, 2021, pp. 1081–1089.
- [45] G. Rios and F. Tobar, “Compositionally-warped Gaussian processes,” *Neural Netw.*, vol. 118, pp. 235–246, Oct. 2019.
- [46] L. Dinh and S. Bengio, “Density estimation using Real NVP,” in *Proc. Int. Conf. Learn. Represent. (ICLR)*, 2017.
- [47] A. Gu and T. Dao, “Mamba: Linear-time sequence modeling with selective state spaces,” in *Proc. First Conference on Language Modeling*, Oct. 2024.
- [48] J. Maroñas and D. Hernández-Lobato, “Efficient transformed Gaussian processes for non-stationary dependent multi-class classification,” in *Proc. Int. Conf. Mach. Learn. (ICML)*, 2023, pp. 24 045–24 081.
- [49] S. Theodoridis, *Machine Learning: A Bayesian and Optimization Perspective*, 2nd ed. Academic Press, 2020.
- [50] Y. Chen, D. Sanz-Alonso, and R. Willett, “Autodifferentiable ensemble Kalman filters,” *SIAM J. Math. Data Sci.*, vol. 4, no. 2, pp. 801–833, 2022.
- [51] G. Evensen, “Sequential data assimilation with a nonlinear quasi-geostrophic model using Monte Carlo methods to forecast error statistics,” *J. Geophys. Res. Oceans*, vol. 99, no. C5, pp. 10 143–10 162, 1994.
- [52] D. P. Kingma and J. Ba, “Adam: A method for stochastic optimization,” in *Proc. Int. Conf. Learn. Represent. (ICLR)*, 2015.
- [53] D. P. Kingma and M. Welling, “An introduction to variational autoencoders,” *Found. Trends Mach. Learn.*, vol. 12, no. 4, pp. 307–392, 2019.
- [54] A. Paszke, S. Gross, F. Massa, A. Lerer, J. Bradbury, G. Chanan, T. Killeen, Z. Lin, N. Gimelshein, L. Antiga *et al.*, “Pytorch: an imperative style, high-performance deep learning library,” in *Proc. Adv. Neural Inf. Process. Syst. (NeurIPS)*, 2019, pp. 8026–8037.
- [55] E. N. Lorenz, “Predictability: A problem partly solved,” in *Proc. Seminar on predictability*, vol. 1, no. 1. Reading, 1996, pp. 1–18.